Calculation of Viscous Hypersonic Flow over a Severely Indented Nosetip

T. Hsieh*
Naval Surface Weapons Center, Silver Spring, Maryland

A numerical procedure for computing viscous hypersonic flows over severely indented nosetips is described. The computer code has been satisfactorily verified for the cases of laminar flow over a hemisphere cylinder with an adiabatic wall at Mach 3 and a sphere cone with an isothermal wall at Mach 6. It is also demonstrated that the code can compute both laminar and turbulent flowfields for a severely indented nosetip with a large separation bubble. Numerical results are presented and compared to experimental data for surface pressure, shock shape, density and velocity fields, and heat transfer in terms of Stanton number.

Nomenclature

a = speed of sound
CN = Courant number
e = total energy per unit volume
j, k = mesh index in ξ and η directions, respectively
J, K = total mesh points in ξ and η directions, respectively
$\mathcal{J}$ = Jacobian of transformation
L = reference length
M = Mach number
$\bar{N}$ = number in time integration
$\bar{n}$ = normal distance
p = pressure
Pr = Prandtl number
q_∞ = freestream velocity
Re = Reynolds number $(\rho_\infty q_\infty L/\mu_\infty)/(\sqrt{\gamma}\, M_\infty)$
S = body arc length
St = Stanton number, $\dfrac{\mu/\mu_\infty}{Re_\infty Pr}\left(\dfrac{T_0}{T_\infty}-\dfrac{T_w}{T_\infty}\right)^{-1}\dfrac{\partial(T/T_\infty)}{\partial(\bar{n}/L)}$
t = time
T = temperature
u, v = velocity components in cylindrical coordinates
x, y = coordinates in the physical plane
β = clustering parameter
γ = ratio of specific heat (Cp/Cv)
ε = internal energy of a gas
$\varepsilon_E, \varepsilon_I$ = explicit and implicit dissipation coefficients, respectively
κ = coefficient of thermal conductivity of a gas
μ = coefficient of viscosity of a gas
ξ, η = coordinates in the computational plane
τ = time after transformation

Subscripts

∞ = freestream condition
w = wall

I. Introduction

In Ref. 1, inviscid calculations of hypersonic flow over a series of indented nosetips were conducted. It was found that for severely indented nosetips the surface pressure predicted by the inviscid calculation differs significantly from the measured data because of flow separation which requires a solution to the viscous flow, or the Navier-Stokes equations.

Presented as Paper 83-0226 at the AIAA 21st Aerospace Sciences Meeting, Reno, Nev., Jan. 10-13, 1983; submitted Jan. 29, 1983; revision received Aug. 19, 1983.

*Aerospace Engineer. Associate Fellow AIAA.

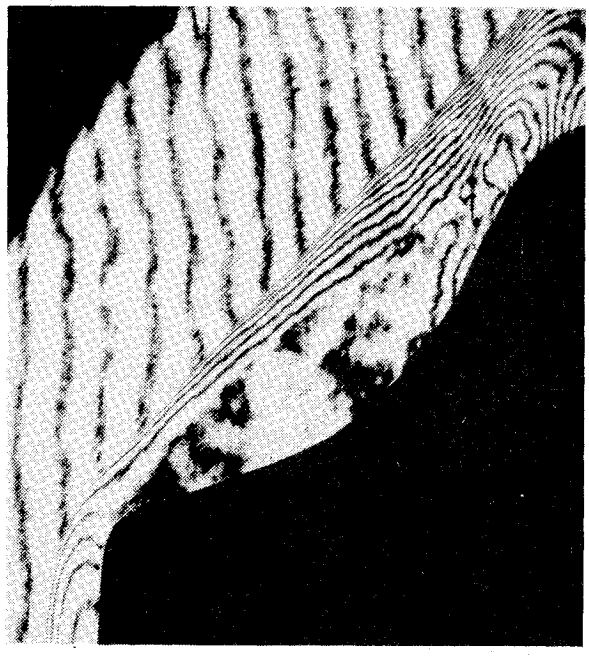

Fig. 1 Hologram of flow over nosetip at $M_\infty = 5$.

The experiment reported in Ref. 2 indicated that the separation bubble can be very large (see Fig. 1) and detailed measurements of the flowfield were given to facilitate future development of a prediction scheme for such a flow problem. Calculations of viscous hypersonic flow over indented nosetips by solving Navier-Stokes equations with thin-layer approximation were reported by Kutler et al.[3] They indicated that the solution for surface temperature of a hemisphere cylinder with adiabatic wall was mesh dependent as given by their code. Using their code, the author encountered two problems: 1) it was not possible to reproduce the results of surface temperature distribution of a hemisphere-cylinder case reported in Fig. 7 of Ref. 3 and 2) when the turbulence model was turned on to compute the flowfield about an indented nosetip, it would not produce a converged solution. This led to a reanalysis of the problem and rewriting of the viscous subroutines including the turbulence model. The revised code eliminates the dubious character of mesh-dependent solutions[4] and also the heat transfer calculation checks very well with a boundary-layer solution for a sphere cone.[4] Also, by detailed comparison, it was possible to pinpoint the error of the original code as described later in Sec. III. In this paper, an effort to compute the viscous hypersonic flow over the specific indented nosetip that was tested and reported in Ref. 2 will be described. Both laminar and turbulent solutions are provided.

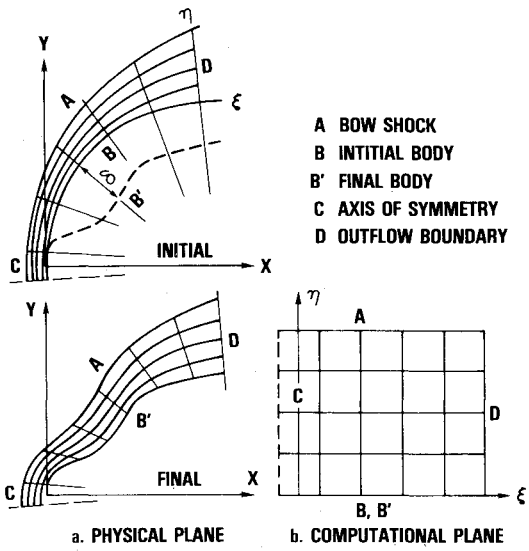

Fig. 2 Coordinate system.

II. Numerical Procedure

The transformed time-dependent compressible Navier-Stokes equations with thin-layer approximation for axisymmetric flows of a perfect gas can be written in the nondimensional and weak conservation law form as follows.

$$q_\tau + E_\xi + F_\eta + H = (1/Re)(S_\eta + T) \tag{1}$$

where a general coordinates transformation (Fig. 2) $\xi = \xi(x, y, t)$, $\eta = \eta(x, y, t)$, $\tau = t$ is used and $q = (1/\mathscr{J}) \times [\rho, \rho u, \rho v, e]^{Tr}$ and E, F, H, S, and T are functions of q.

The numerical algorithm used to solve Eq. (1) is the implicit, approximately factored finite difference algorithm in delta form as described by Beam and Warming.[7] Using the Euler implicit time differencing, the final difference equations may be split into two sets of one-dimensional equations in the computational directions ξ and η as follows:

$$\begin{aligned}&\left[I + \Delta\tau\delta_\xi \tilde{A}^n - \varepsilon_I\left(\mathscr{J}^{-1}\nabla_\xi\Delta_\xi\mathscr{J}\right)^n\right]\Delta q^{*n} \\ &= -\Delta\tau\left[\delta_\xi E^n + \delta_\eta F^n + H^n - \frac{1}{Re}\left(\delta_\eta S^n + T^n\right)\right] \\ &\quad - \frac{\varepsilon_E}{8}\left(\mathscr{J}^n\right)^{-1}\left[\left(\nabla_\xi\Delta_\xi\right)^2 + \left(\nabla_\eta\Delta_\eta\right)^2\right]\left(\mathscr{J}q\right)^n \end{aligned} \tag{2a}$$

$$\begin{aligned}&\left[I + \Delta\tau\delta_\eta\left(\tilde{B} - \frac{\tilde{M}}{Re}\right)^n - \frac{1}{Re}\delta_{\eta\eta}\tilde{Q}^n + \tilde{K}^n\right. \\ &\left. - \frac{1}{Re}\left(\tilde{N} - \delta_\eta\tilde{W}\right)^n - \varepsilon_I\left(\mathscr{J}^{-1}\nabla_\eta\Delta_\eta\mathscr{J}\right)^n\right]\Delta q^n = \Delta q^{*n}\end{aligned} \tag{2b}$$

where $\tilde{A}$, $\tilde{B}$, $\tilde{K}$, $\tilde{M}$, $\tilde{N}$, $\tilde{Q}$, and $\tilde{W}$ are the Jacobian matrices and can be found in Ref. 6, and I is the identity matrix. δ_ξ and δ_η are second-order central difference operators, and ∇ and Δ represent the conventional forward and backward difference operators. The terms led by ε_I and ε_E are the implicit and explicit dissipation terms. Equations (2a) and (2b) are applied to the interior points in the computation domain and give a block (4×4) tridiagonal system of equations which can be solved by the LU-decomposition method. The differences in the revised code are the viscous terms given in Eq. (2b), which are casted differently for clarity (Ref. 6 contains detailed derivation of the equations and a listing of the code, except the turbulence model subroutine).

As shown in Fig. 2, the flowfield of interest is enclosed by the four boundaries A, B, C, and D where A is the bow shock, B the body surface, C the axis of symmetry, and D the outflow plane. The shock fitting scheme described by Kutler[3] remains unchanged. Since the explicit method is used in the shock boundary, the time step $\Delta\tau_s$ for shock integration is restricted by the CFL condition. In order to have a time-accurate calculation, the time step used for the integration of the interior points must also not exceed $\Delta\tau_s$. As a result, the Courant number for a time-accurate calculation is limited to about 70 in most calculations reported in this paper. On the body surface, the no-slip boundary condition is imposed explicitly. The surface pressure is determined from the following relation since at the body surface the normal pressure gradient is zero:

$$p_n = \frac{1}{\left(\eta_x^2 + \eta_y^2\right)^{\frac{1}{2}}}\left[\left(\xi_x\eta_x + \xi_y\eta_y\right)p_\xi + \left(\eta_x^2 + \eta_y^2\right)p_\eta\right] = 0 \tag{3}$$

Similarly, for the adiabatic wall boundary condition, the temperature may be determined by

$$\left(\xi_x\eta_x + \xi_y\eta_y\right)T_\xi + \left(\eta_x^2 + \eta_y^2\right)T_\eta = 0 \tag{4}$$

For the isothermal wall boundary condition, the wall temperature is held constant throughout the entire convergence process. Once the pressure and the temperature are known, the density is determined from the equation of state. The plane of symmetry, boundary C, is enforced implicitly using the reflection principle by choosing the first two $\xi = \text{const}$ lines to straddle the axis; and, in the outflow plane, a linear extrapolation of all the flow variables is imposed. To start the calculation, an initial flowfield must be provided. In this paper, the calculation always starts from an inviscid flowfield of a sphere cone.

A two-layer algebraic eddy viscosity model of Ref. 5 is applied in the conventional manner. That is,

$$(\mu_t)_{\text{inner}} = \rho(0.4D\bar{n})^2|\omega| \tag{5a}$$

$$(\mu_t)_{\text{outer}} = 0.02688F_{\text{wake}}F_{\text{kleb}}(\bar{n}) \tag{5b}$$

where the normal distance from the wall $\bar{n}$ was used. Details of the model can be found from Ref. 5. In the calculation, μ is replaced by $(\mu + \mu_t)$ and κ/Pr (note: $\kappa/\kappa_\infty = \mu/\mu_\infty$) is replaced by $[(\mu/Pr) + (\mu_t/Pr)]$. In Ref. 3, Kutler et al. mentioned that a very large implicit dissipation coefficient (as large as 6) was required in order to do turbulent flow calculation. For the turbulent flow over indented nosetip calculation to be described later, ε_I is not required, i.e., $\varepsilon_I \equiv 0$.

III. Results and Discussion

Numerical results have been obtained for three cases: 1) laminar flow over a hemisphere cylinder with an adiabatic wall at $M_\infty = 2.94$, $Re_\infty = 2.2 \times 10^5$, and $T_0 = 293$ K; 2) laminar and turbulent flows over a sphere cone with an isothermal wall ($T_w/T_\infty = 4.4$) at $M_\infty = 5.92$ and $Re_\infty = 10^6$; and 3) laminar and turbulent flows over a severely indented nosetip with an isothermal wall ($T_w/T_\infty = 5.4$) at $M_\infty = 5$ and $Re_\infty = 2.64 \times 10^7$/m. These results will be described and discussed in the following paragraphs.

Hemisphere Cylinder

Laminar flow over a hemisphere cylinder is chosen as a case for verification of the revised code. The steady-state convergence criterion used in present calculations is the nondimensional shock speed (normalized by $a_\infty/\sqrt{\gamma}$) which, from experience, must be in the order of 10^{-3}. In Fig. 3 the results of surface temperature distribution with three different meshes (see Table 1) by varying the clustering factor β in the normal

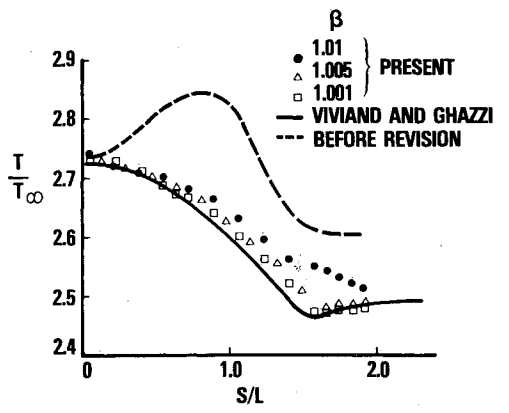

Fig. 3 Surface temperature distribution for hemisphere cylinder with adiabatic wall at $M_\infty = 2.94$, $Re_\infty = 2.2 \times 10^5$, and $T_0 = 293$ K.

Table 3 Temperature distribution for hemisphere cylinder at $M_\infty = 2.94$, $Re_\infty = 2.2 \times 10^5$, and $T_0 = 293$ K

Arc length	T/T_∞ Mesh B	T/T_∞ Mesh C
0.042	2.733	2.731
0.212	2.724	2.725
0.382	2.712	2.712
0.552	2.693	2.693
0.722	2.670	2.667
0.891	2.641	2.637
1.061	2.607	2.600
1.231	2.572	2.562
1.400	2.530	2.521
1.570	2.486	2.472
1.740	2.480	2.474
1.910	2.483	2.476

direction from 1.01 (mesh A) to 1.005 (mesh B) and to 1.001 (mesh C) are shown. Table 2 gives the nondimensional shock speed at the end of time integration. It is seen that the results obtained from meshes B and C (tabulated in Table 3) agree quite well but not those given by mesh A which does not provide enough points near the surface to resolve the viscous effects. Also, shown in Fig. 3 is the solution of Viviand and Ghazzi[8] and a slight difference is shown in the area near the shoulder between their solution and the present one. The author was unable to reproduce the results of mesh-dependent temperature distribution of Kutler et al. as given in Fig. 7 of Ref. 3 from the copy of the computer code obtained from them. The result of T/T_∞ given by Kutler's code using mesh B is shown in the dotted line. A detailed comparison reveals that an error was made in the viscous portion of the energy equation in the original code.[9] After correction of the error, it was able to produce the same result given by the revised code as shown in Fig. 3. It should be pointed out that the solutions for shock shape and surface pressure are not sensitive to the error made in the energy equation.

Sphere Cone

A further verification of the revised code is made for the case of heat transfer calculation for laminar flow over a sphere cone to compare the thin-layer solution with the boundary-layer solution using the numerical code of Cebeci et al.[10] Since no flow separation is likely to occur for this case, one would expect good agreement between the two solutions. In the boundary-layer calculation, the surface pressure must be given. In order to have a reasonable comparison, the surface pressure calculated from the thin-layer theory was used in the boundary-layer calculation. The calculated results (using a mesh of $J \times K = 28 \times 32$ with $\beta = 1.005$) of heat transfer distribution in terms of Stanton number over the surface are shown in Fig. 4. The agreement is indeed very good from the tip up to the juncture of the sphere and the cone, and from there on slightly higher heat transfer is predicted by the thin-layer theory. Table 4 gives the computed values of St vs arc length for two different values of ε_E of 0.1 and 0.02. The influence of ε_E in this case is insignificant. It should be pointed out that the surface pressure calculated from the thin-layer theory also agrees quite well with an inviscid solution[4] and the measured heat transfer data for this case are scattered over a large range; thus, it should not be used to assess a numerical solution.

Also shown in Fig. 4 is the turbulent solution. It is seen that the heat transfer increases significantly when the flow is turbulent everywhere. The turbulent solution for surface pressure remains essentially the same as in the laminar solution.

Indented Nosetip

The configuration of the indented nosetip as shown in Fig. 1 can be found in Ref. 1 or 2. Because of the strong variation in

Table 1 Mesh

Mesh	β	Points within $0.1Ys$	$J \times K$	First 6 points $\bar{n}_2/Ys$[a]	$\bar{n}_3/Ys$	$\bar{n}_4/Ys$	$\bar{n}_5/Ys$	$\bar{n}_6/Ys$	$\bar{n}_7/Ys$
A	1.01	12	25×25	0.0025	0.0055	0.0093	0.014	0.0199	0.0271
B	1.005	17	25×32	0.0011	0.0024	0.0039	0.0058	0.0081	0.0109
C	1.001	20	25×32	0.0003	0.0006	0.0011	0.0017	0.0024	0.0033

[a] $\bar{n}_k/Ys = 1 + \beta(1 - \alpha^{b''})/(1 + \alpha^{b''})$ where $\alpha = \dfrac{\beta + 1}{\beta - 1}$ and $b'' = 1 - \dfrac{(k-1)}{(K-1)}$.

Table 2 Shock speed

Mesh	Number of time integrations	Shock speed	Remarks
A	400	0.26×10^{-5}	a) $CN = 75$ and final $\varepsilon_E = 0.02$ and $\varepsilon_I \equiv 3\varepsilon_E$ for all cases
B	600	0.5×10^{-5}	b) Mesh C starts with $\varepsilon_E = 0.1$ and $CN = 25$ for 400 steps and the convergence becomes very slow
C	1600	0.54×10^{-5}	

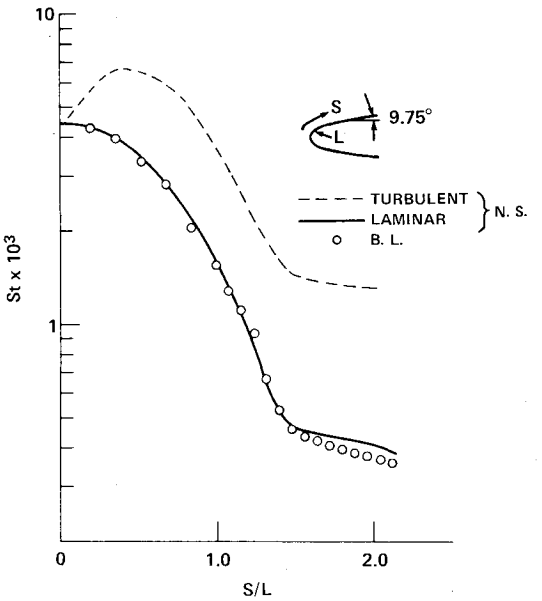

Fig. 4 Heat transfer distribution in terms of Stanton number for sphere cone with isothermal wall of $T_w/T_\infty = 4.4$ at $M_\infty = 5.92$ and $Re_\infty = 10^6$.

Table 4 Stanton number distribution for sphere cone at $M_\infty = 5.92$, $Re_\infty = 10^6$, $T_w/T_\infty = 4.4$

	$St \times 10^2$	
Arc length	S_s[a] $= 0.5 \times 10^{-3}$, $\varepsilon_E = 0.1$	$S_s = 0.1 \times 10^{-3}$, $\varepsilon_E = 0.02$
0.04	0.445	0.438
0.20	0.430	0.430
0.36	0.396	0.395
0.52	0.345	0.345
0.68	0.284	0.284
0.84	0.220	0.220
1.0	0.159	0.160
1.16	0.108	0.107
1.32	0.066	0.066
1.48	0.046	0.046
1.64	0.044	0.044
1.80	0.042	0.042
1.96	0.040	0.039

[a] S_s = nondimensional shock speed.

surface curvature, considerable difficulties were encountered in obtaining a converged solution for the inviscid flow calculation reported in Ref. 1. A special calculation procedure of successive approximation of the body geometry by adding mesh points in the process of convergence of a solution was developed in Ref. 1, and reasonable solutions were obtained. The similar calculation procedure is also needed in the calculation of viscous flow but it is much easier to carry out than in the inviscid flow calculations. In the viscous flow calculation of the nosetip shown in Fig. 1, a starting mesh of $J \times K = 20 \times 32$ for a sphere cone was used to do laminar calculation. The mesh was evenly distributed in the streamwise direction but was clustered with $\beta = 1.005$ in the k direction. The code can automatically deform the body from the sphere cone (easier to set up the initial flowfield) to the desired nosetip shape in a specified number of time steps. For this case it took 2800 time steps to complete the deformation (about 6.5 min CRAY CPU time). The subsequent mesh increases were 36×32, 50×32, 59×32, and 68×32. Each took 400 time steps to establish the flowfield (total 10.7 min CRAY CPU time). At this point, it seems that the mesh distribution is sufficient. (See Fig. 7 for mesh distribution along the surface. An increase of

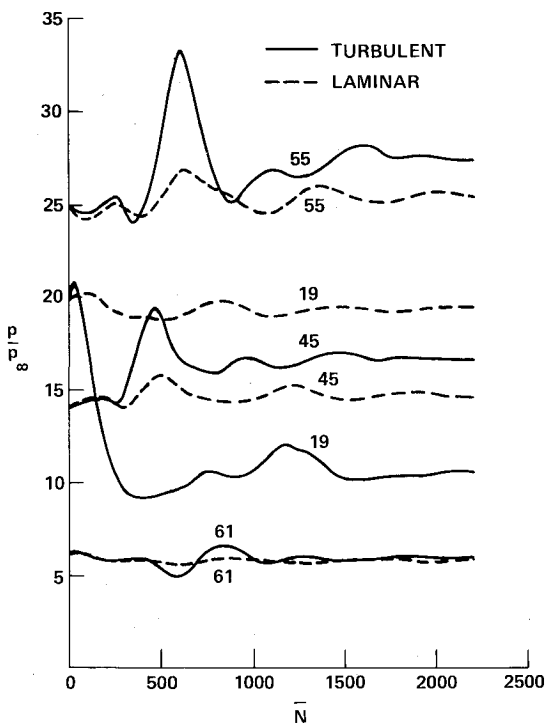

Fig. 5 Convergence of surface pressure.

mesh in the η direction from 32 to 48 and continuing the run for 200 time steps showed no overall change in the results.)

The laminar flowfield obtained at this stage gave an average shock speed of 0.07 and maximum shock speed of 0.18, thus it cannot be considered a converged solution. Instead, the obtained flowfield was used as the starting flowfield in the process of obtaining a converged solution for both laminar and turbulent flow calculations. In this way, the convergence process for laminar and turbulent flows can be compared. In addition, it has been pointed out[11,12] that for a severely indented nosetip, it is possible to have a self-excited oscillating flow. For that reason, it is necessary to keep the calculation time accurate by limiting the Courant number to 50 for both turbulent and laminar calculations. Furthermore, in order to reduce the effects of explicit dissipation used in the algorithm on the true viscous effects near the body surface, a reduction of the ε_E value from the given value of 0.3 at the shock where the flow is essentially inviscid to about 0.03 at the surface according to the following expression

$$\varepsilon_E = 0.3\left[0.9(k/K)^2 + 0.1\right] \tag{6}$$

has been incorporated into the code. A plot of the convergence of the solution for surface pressure at four locations is shown in Fig. 5. It is seen that although the turbulent flow case shows large transient variation as one would expect, it reaches the steady state faster than the laminar flow case. The laminar flow has not quite reached the steady state yet but the trend indicates there is a steady state. Therefore, no self-excited oscillating flow occurs for this specific nosetip and flow conditions under investigation. At the end of $\bar{N} = 3000$, the average shock speeds are 0.0012 and 0.0019 and the maximum shock speeds are 0.0023 and 0.0045 for turbulent and laminar flow solutions, respectively. A description and comparison of the calculated laminar and turbulent flowfields and the experimental data are given in the following paragraphs.

In engineering applications, a primary concern is how well the surface pressure can be predicted. A plot of surface pressure along the body arc length is shown in Fig. 6 for laminar and turbulent solutions and the experimental data.

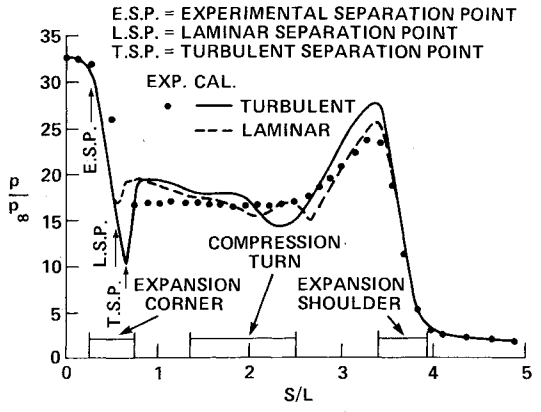

Fig. 6 Comparison of surface pressure distribution for indented nosetip, $T_w/T_\infty = 5.4$, $M_\infty = 5$, and $Re_\infty = 2.64 \times 10^7/\text{m}$.

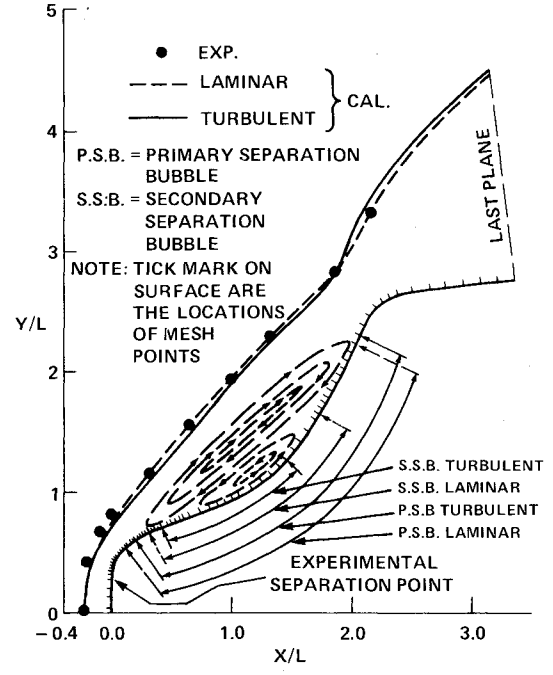

Fig. 7 Comparisons of shock locations and separation points and sketch of the computed flowfield for indented nosetip, $T_w/T_\infty = 5.4$, $M_\infty = 5$, $Re_\infty = 2.64 \times 10^7/\text{m}$.

The striking differences among the solutions and the experiment are the locations of flow separation and, hence, the surface pressure there. The turbulent flow separates slightly downstream of the laminar separation point as one would expect. However, the fact that both the laminar and the turbulent separation points are located far downstream of the experimental separation point, which is at the beginning of the expansion corner, is difficult to explain. In Ref. 1, the effective body concept, which matches the calculated inviscid surface pressure with the experimental data, indicates that the flow is indeed separated at the very beginning of the expansion corner. However, the circumferential surface pressure measurements at stations $x = 3.189$ and 4.773 (see Ref. 2) reveal possible flow angularity in the wind tunnel. If the flow angularity causes the nose to go up slightly (positive angle of attack), then the separation point will move forward since laminar flow is very easy to separate. Before flow separation, the laminar and turbulent solutions (also the inviscid solution, not shown) coincide but are much lower than the experimental data. It is likely that the real flow changes from laminar to turbulent around the expansion corner; therefore, one needs a better turbulence model that can cope with transitional flow in

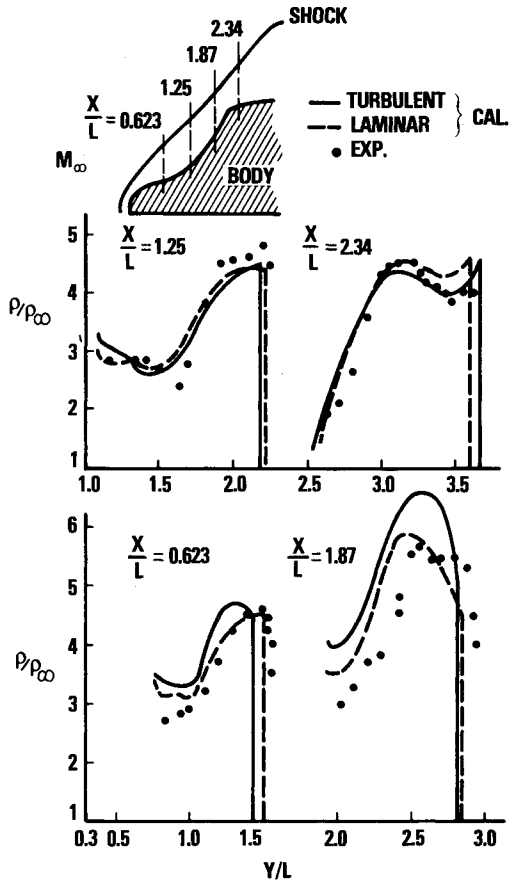

Fig. 8 Comparison of density distribution for indented nosetip, $T_w/T_\infty = 5.4$, $M_\infty = 5$, $Re_\infty = 2.64 \times 10^7/\text{m}$.

order to improve the calculation. The peak pressure occurs at the region where the flow reattaches and is seen to agree well in location but not in magnitude among the solutions and the experiment. In the separated region, the measured data indicate that the pressure there is essentially constant over a large portion of the region and steadily increases afterward, but the solutions show more variation of surface pressure in the same region. After the flow reattaches, good agreement between the numerical results and the experimental data is shown in Fig. 6.

Figure 7 shows the shock location obtained from the laminar and turbulent solutions and the experiment and a sketch of the flowfield within the separation bubble. Also shown in Fig. 7 are the locations of mesh points on the body surface. The reason for more concentrated mesh points near the expansion corner is to resolve the separation point. Since the predicted separation points are farther downstream than the experimental one, the shock layer there is thinner than the measured one. Downstream of the separation point, the laminar solution agrees better with the measured data than the turbulent solution. In both solutions, there is a secondary separation bubble around the compression turn. It is difficult to assess how real the secondary separation is because the velocity measurements, as described later, did not come close enough to the wall to detect the reverse in flow direction for the secondary bubble. From the comparison made in Figs. 6 and 7, the laminar solution agrees better with the experiment, in general.

Figure 8 shows the comparison of density distribution in the plane of $x/L = 0.623$, 1.25, 1.87, and 2.34 and between the numerical solutions and the measured data deduced by Wardlaw[13] of NSWC. It should be pointed out that the data given in Ref. 2 for $S/L = 2.318$ were not deduced correctly. In general, the agreements are satisfactory except at station $x/L = 1.87$ where the data seem shifted to the right.

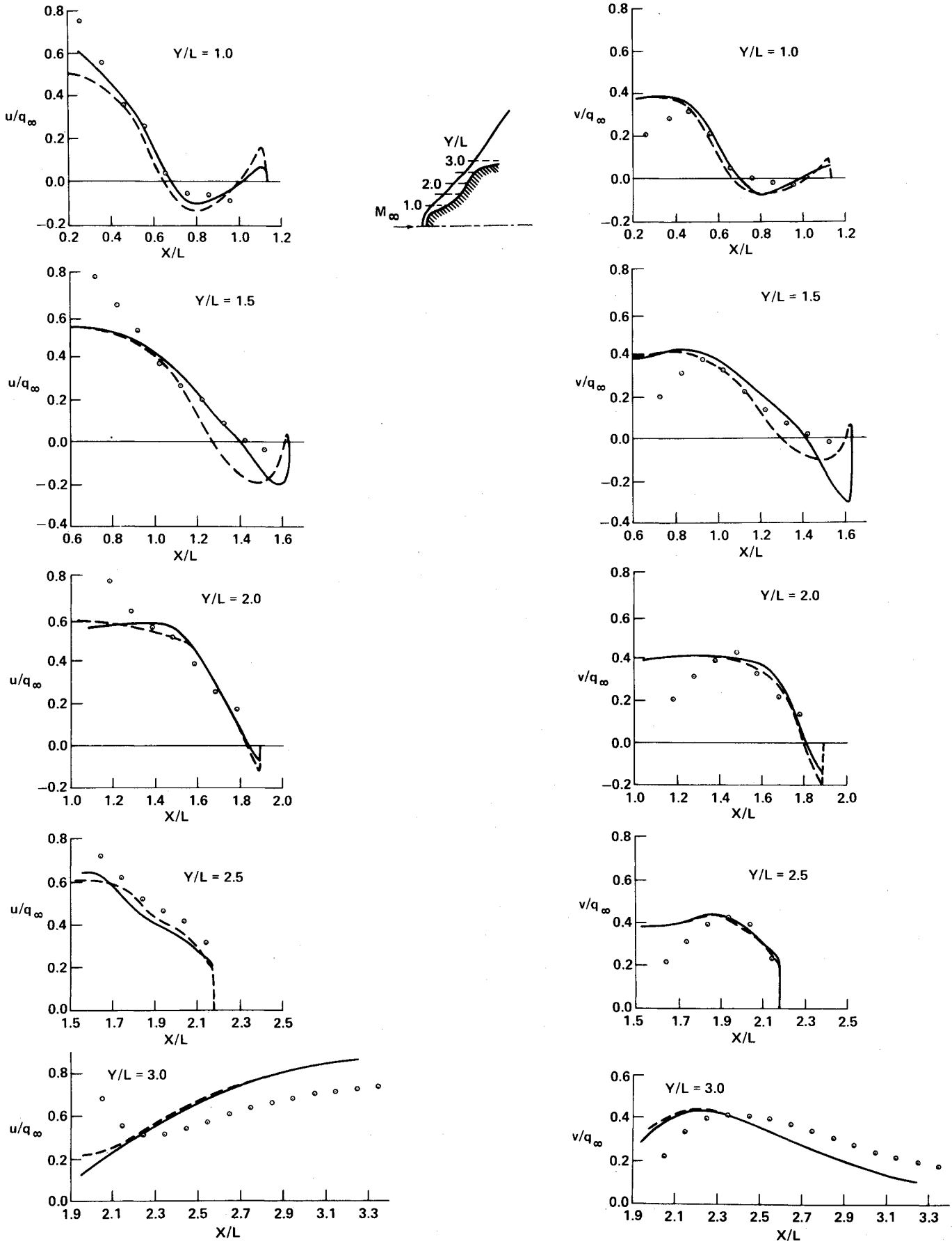

Fig. 9 Comparison of velocity distribution for indented nosetip, $T_w/T_\infty = 5.4$, $M_\infty = 5$, $Re_\infty = 2.64 \times 10^7/\text{m}$.

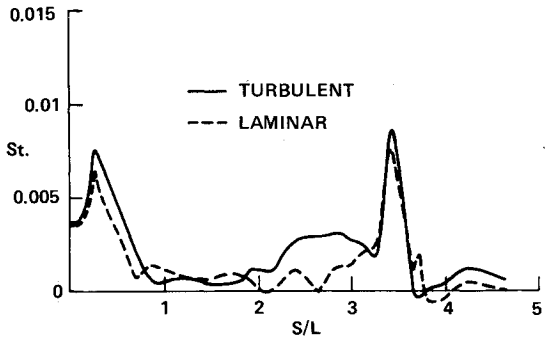

Fig. 10 Distribution of heat transfer in terms of Stanton number for indented nosetip, $T_w/T_\infty = 5.4$, $M_\infty = 5$, $Re_\infty = 2.64 \times 10^7/\text{m}$.

Figure 9 shows the comparison of velocity distribution at $Y/L = 1.0$, 1.5, 2.0, 2.5, and 3.0 planes (note: the velocity data published in Ref. 2 must be corrected by a factor of 3.28). As the authors described in Ref. 2, it is possible that the LDV data suffered some degree of particle lag problem. Figure 9 confirms that this is the case. The u component near the shock is always higher than the numerical value and the v is always less. It is difficult to evaluate how far away from the shock the lag problem disappears for all the data shown. Nevertheless, the general trend of the measured data agrees with the numerical solutions. At stations $Y/L = 1.0$ and 1.5 (for laminar flow only) the existence of secondary separation near the body surface is indicated by the twice reverse of flow direction as shown by the calculation. Unfortunately, there is no experimental data there to verify if this is true.

Figure 10 shows the numerical results for heat transfer in terms of Stanton number. There are two peaks in the heat transfer distribution, one is near the corner and the other is on the fore portion of the shoulder, where the flow reattaches. There are locations where the heat transfer rate becomes an order smaller or even negative. It must be pointed out that in these locations the calculated St values may vary from 5 to 10% in a few hundred time steps while the temperature field itself only varies about 0.05% (note, St depends on temperature gradient). The calculated St values between $S = 0.3$ and 1.0 also oscillate somewhat and averaged values were used as shown in Fig. 10. No heat transfer data is available for comparison.

From the preceding description and comparison of the results, it is clear that the current computer code can provide a reasonable solution for the type of flowfield under investigation. However several areas require improvement:

1) The final mesh near the expansion corner may be too far away from normal to the body surface. It would be better if an approximately orthogonal mesh was introduced after the body has been deformed to the desired configuration.

2) A semiautomatic adding of mesh should be incorporated in the code to reduce human interaction with the calculation to a minimum.

3) An implicit shock fitting[14] and body boundary condition should be implemented to speed up the convergence process and increase the size of time step.

4) A better turbulence model, including the capability of handling transitional flow, should be introduced since it is obvious that the flow is laminar near the tip blunt region and changes to turbulent at a downstream location.

5) The validity of thin-layer theory to compute a flow with a large separation bubble as shown in Fig. 1 is generally questionable. On the other hand, it is also not practical to have a mesh of $\Delta x \sim \Delta y$ such that the streamwise dissipation terms can be effectively resolved. Therefore, the only thing one can do is to program the full Navier-Stokes equations and check the thin-layer solution against the solution of the full Navier-Stokes equations under the affordable mesh points when one feels necessary. After completion of the work reported the code has been vectorized and the vectorized code runs 2.43 times faster using the same CRAY computer.

IV. Concluding Remarks

A numerical simulation of viscous hypersonic flows over indented nosetips is described. The computer code has been satisfactorily verified for the cases of laminar flow over a hemisphere cylinder with an adiabatic wall at Mach 3 and a sphere cone with an isothermal wall at Mach 6. It is also demonstrated that the code can compute both laminar and turbulent (using eddy viscosity model) flowfields for a severely indented nosetip with a large separation bubble as shown in Fig. 1 at Mach 5. Areas of improvement of the code are suggested.

Acknowledgment

Part of the work was sponsored by the Fluid Mechanics Program of the Naval Air Systems Command monitored by D.E. Hutchins. The boundary-layer calculation was provided by Dr. W. Ragsdale of NSWC. The CRAY computer time was provided by NASA Ames Research Center, Applied Computational Fluid Dynamics Branch, through a cooperation program.

References

[1]Hsieh, T., "Calculation of Hypersonic Flows Over a Series of Indented Nosetips," *Journal of Spacecraft and Rockets*, Vol. 19, May-June 1982, pp. 193-194; also, AIAA Paper 81-0077, 1981.

[2]Morrison, A.M., Yanta, W.J., and Voisinet, R.L.P., "The Hypersonic Flow Field Over a Re-entry Vehicle Indented Nose Configuration," AIAA Paper 81-1060, June 1981.

[3]Kutler, P., Chakravarthy, S.R., and Lombard, C.P., "Supersonic Flow Over Ablated Nosetips Using an Unsteady Implicit Numerical Procedure," AIAA Paper 78-213, Jan. 1978.

[4]Hsieh, T., "Heat Transfer Calculation for Hypersonic Flows Over Blunt Noses Using an Unsteady Implicity Scheme," *Proceedings of the Second National Symposium on the Numerical Methods in Heat Transfer*, Hemisphere Publishing Corp., Washington, D.C., 1982, pp. 375-401.

[5]Baldwin, B.S. and Lomax, H., "Thin-layer Approximation and Algebraic Model for Separated Turbulent Flows," AIAA Paper 78-257, Jan. 1978.

[6]Hsieh, T., "Calculation of Flowfield about Indented Nosetips," Naval Surface Weapons Center TR 82-286, Dec. 1982.

[7]Beam, R.M. and Warming, R.F., "An Implicit Factored Scheme for the Compressible Navier-Stokes Equations," *AIAA Journal*, Vol. 16, April 1978, pp. 393-402.

[8]Viviand, H. and Ghazzi, W., "Numerical Solution of the Navier-Stokes Equations at High Reynolds Numbers with Application to the Blunt Body Problem," *Lecture Notes in Physics No. 59, Proceedings of the Fifth International Conference on Numerical Methods in Fluid Dynamics*, 1976, pp. 434-439.

[9]Hsieh, T., private communication with P. Kutler, July 6, 1983.

[10]Cebeci, T., Mosinskis, G., and Wang, L.C., "A Finite Difference Method for Calculating Compressible Laminar and Turbulent Boundary Layers: Part I and II," DAC-67131, McDonnell Douglas Aircraft Company, May 1969.

[11]Hankey, W.L. and Shang, J.S., "Analysis of Self-Excited Oscillations in Fluid Flows," AIAA Paper 80-1346, July 1980.

[12]Widhopf, G.F. and Vectoria, K.J., "Numerical Solution of the Unsteady Navier-Stokes Equations for the Oscillatory Flow Over a Concave Body," Lecture Notes in Physics, No. 35, *Proceedings of the Fourth International Conference on Numerical Methods in Fluid Dynamics*, June 1974, pp. 431-444.

[13]Wardlaw, A.B. Jr., private communication.

[14]Chakravarthy, S.R., "Euler Equations-Implicit Schemes and Boundary Conditions," *AIAA Journal*, Vol. 21, May 1983, pp. 699-706.